Biomedical Signal Processing and Control 115 (2026) 109444

Contents lists available at ScienceDirect

Biomedical Signal Processing and Control

journal homepage: www.elsevier.com/locate/bspc

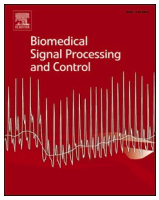

Generalised oedema monitoring utilising a NIR hyperspectral camera in critically ill neonates: A feasibility study

Mariana Castro-Montano [a,*], Andy Petros [b], Ling Li [a], Enayetur Rahman [a], Simon Hannam [b], Grant Clow [a], Panayiotis A Kyriacou [a], Jim McLaughlin [c], Meha Qassem [a]

[a] Research Centre for Biomedical Engineering, City St George's, University of London, London, UK
[b] Paediatric and Neonatal Intensive Care Units, Great Ormond Street Hospital (GOSH), London, UK
[c] NIBEC, School of Engineering, Ulster University, UK

ARTICLE INFO

Keywords:
Generalised oedema
Spectroscopy
Near infrared light
PLS-DA

ABSTRACT

Generalised oedema is common in neonatal intensive care units (NICUs), particularly in preterm and low-birth-weight infants. Characterised by tissue swelling from excess water accumulation, it can reflect systematic illness such as congestive heart failure, hepatic cirrhosis, nephrotic syndrome, sepsis, and acute kidney injury. Current clinical assessment methods, including formulas based on weight and fluid input/output and visual skin observation, lack accuracy and sensitivity, especially in critically ill infants. Techniques such as bioimpedance and ultrasound have been explored but are unsuitable for neonates and do not provide direct water content measurements. Spectroscopy, a non-invasive optical method, offers a promising solution by measuring tissue water content through light interactions in the Near Infrared (NIR) spectrum. This study investigates oedema in neonates using an NIR hyperspectral system in the NICU. Data was collected from 20 neonates, both with and without oedema over the course of three consecutive days. Spectral analysis revealed significant differences, notably at water absorption peaks around 1200 nm ($p = 0.012$). A Partial Least Squares Discriminant Analysis (PLS-DA) model effectively differentiated between oedematous and non-oedematous infants using spectral and standard clinical features, achieving 85.56 % recall and 100 % precision in testing. These findings suggest NIR spectroscopy combined with PLS-DA offers a reliable, non-contact method for early oedema detection in neonates, potentially enhancing monitoring and outcomes in the NICU.

1. Introduction

Newborns are born with a high proportion of body water, particularly in the extracellular space [1]. Term newborns have approximately 80 % of their body weight as water, while this rises to about 85 % in preterm newborns [2], compared to around 60 % in adults [3]. This excess of fluid leads to a natural fluid loss and an expected weight loss of up to 10 % in the days following birth [4,5]. However, in unwell neonates, this natural fluid loss may be disrupted, making fluid management and requirements particularly challenging [6]. Generalised oedema, characterized by skin swelling due to water accumulation in tissues, is common among neonates in intensive care units [7], particularly those with low birth weight or preterm births [2,5] or underlying conditions including congestive heart failure, hepatic cirrhosis, nephrotic syndrome, sepsis, and acute kidney injury [7]. Oedema can lead to clinical consequences, including deficient tissue perfusion and oxygenation [8], an increased risk of infections through the skin [9], and low levels of serum sodium and albumin [10,11].

Current clinical methods for oedema assessment rely on weight-based formulas, fluid input–output measurements [12], and visual assessment of the skin [7]. However, critically ill neonates may be too unstable to weigh daily, and quantifying fluid outputs such as urine, stool, or vomit is often impractical [6]. As a result, visual assessment remains a common practice, but it is subjective, highly reliant on clinician experience, and lacks sensitivity for early detection.

To address these challenges, non-invasive and bedside techniques such as bioimpedance [13,14] and ultrasound [15,16] have been explored for oedema detection. While promising, these methods are generally unsuitable for critically ill neonates and do not directly measure water content [14,17]. Advanced methods such as air displacement plethysmography (ADP) [18], magnetic resonance imaging (MRI) [19], and dual-energy X-ray absorptiometry (DXA) [20] can provide

* Corresponding author.
E-mail address: Mariana.castro-montano@citystgeorges.ac.uk (M. Castro-Montano).

https://doi.org/10.1016/j.bspc.2025.109444
Received 24 April 2025; Received in revised form 5 November 2025; Accepted 18 December 2025
Available online 22 December 2025

comprehensive body composition metrics, such as fat and fat-free mass. However, these techniques cannot specifically quantify water content and often require neonates to be moved to specialized equipment, posing logistical and safety challenges [21].

This paper reports the first proof-of-principle of a novel, non-invasive and contact-free method for precise detection and monitoring of oedema using spectroscopy in the near-infrared (NIR) region. A hyperspectral camera was used in spectroscopy mode, and no spatial scanning was performed, to rapidly acquire hundreds of spectra across the NIR range. A hyperspectral camera utilizes the interaction of light with tissue across a broad range of wavelengths to generate large amounts of spectra in a short acquisition time without requiring physical contact with the patient [22,23]. A typical NIR spectrum of human skin is characterized by various bands associated to absorption of light by OH, CH and NH functional groups. Strong absorption bands of OH which can be directly linked to dermal water content [24], are observed within the NIR region at 970, 1200, 1450 and 1900 nm [25–27]. Therefore, a hyperspectral camera with near-infrared light could be a potential tool to quantify water within the tissue and thus oedema.

2. Materials and methods

2.1. Sensor and setup

Data was acquired with the Specim FX17e hyperspectral camera (Spectral Imaging Ltd., Oulu, Finland), which operates within the near-infrared spectrum, covering a range of 900–1700 nm with a spectral resolution of 3.5 nm across 224 wavelengths. The camera employs a line-scan approach, where it scans line-by-line along one axis to construct a hyperspectral image. To generate a full image, the camera needs to move at a specific speed. In this application, motorizing the camera was not feasible at this stage of the project. Consequently, rather than capturing a full hyperspectral image, the acquisition was limited to line-scans of the target area, focusing on a single dimension of the scene to avoid disturbing the neonate while still gathering essential spectral data.

For illumination, two halogen light sources (HL-2000, power 20 W, Ocean Optics, Orlando, FL, USA) were employed. Both light sources were connected to optical fibres, ensuring precise and consistent lighting. A custom-made holder (1.92 m × 0.96 m × 1.04 m) was constructed to support the system (Fig. 1). This holder allows for flexible movement of the camera in multiple directions and angles, enhancing the adaptability of the setup. The light sources are securely attached to the holder via the optical fibres, ensuring stable illumination during data acquisition. The system can be positioned easily and safely above the patient without causing disturbance, ensuring a non-invasive and patient-friendly recording process. The camera is connected to a laptop via a Camera Link connector, which enables highspeed data transfer and visualizing the data acquired in real time. For all acquisitions, the integration time was fixed at 45 ms. To calibrate reflectance, dark (0 %) and white (100 %) reference curves were used; these are available in the supplementary material (See supplementary material).

2.2. Data collection

Ethics approval was obtained to conduct the study in the Neonatal Intensive Care Unit (NICU) at Great Ormond Street Hospital (GOSH), London. Hyperspectral data was collected from neonates with and without signs of oedema, as determined by the attending clinician using visual assessments of the skin. Data collection was performed after obtaining consent from the patient's legally authorized representatives. The data was planned to be acquired over three consecutive days at the same time each day. Additionally, standard clinical features were taken from the patient's electronic data record, including weight, birth weight, fluid input and fluid output. During data collection, the camera was positioned at a measured distance of 12 to 15 cm above the abdomen, with the area being illuminated by halogen light

2.3. Data processing

Initial data processing was conducted using MATLAB as illustrated in Fig. 2. The first step involved manually selecting the region of interest

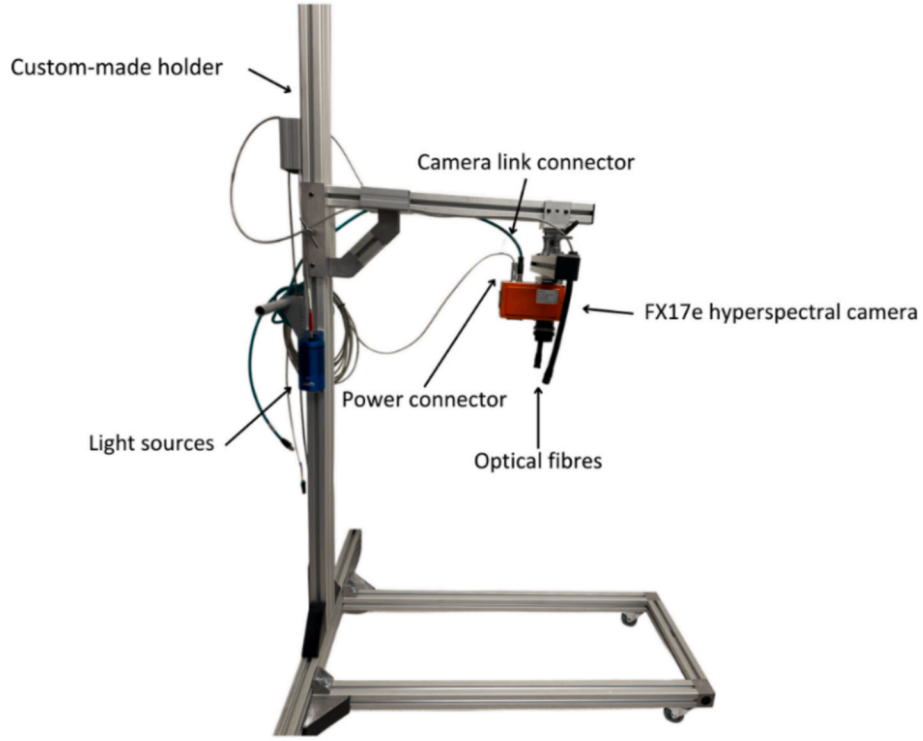

Fig. 1. Hyperspectral system setup.

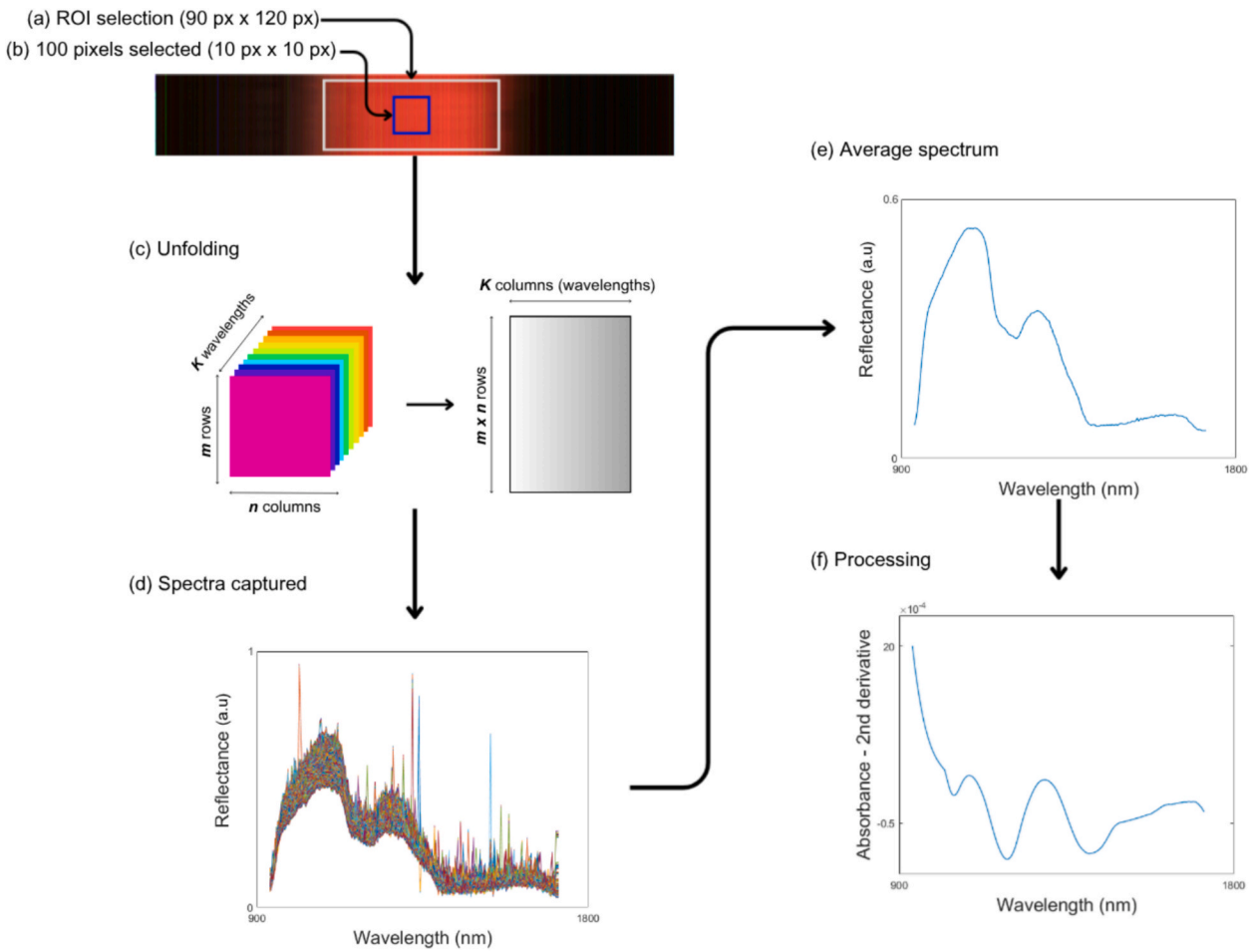

Fig. 2. Data pre-processing. (a) Manual selection of the ROI, focusing on the brightest areas of the image. (b) Extraction of 100 pixels from each image to build datasets for modelling, pixel size is 8 × 16 μm. (c) Unfolding process to transform the 3D data into a 2D format. (d) Spectra obtained from the selected ROI in (a). (e) Calculation of the average spectrum from the extracted spectra. (f) Final processed spectrum.

(ROI), specifically focusing on the bright area that corresponded to the patient's abdomen. Since the data had a 3D structure, the data was unfolded to get a 2D structure to simplify subsequent analysis. This unfolding process preserved the integrity of the data since the camera remained stationary, and no spatial features were captured, only the spectral features of relevance. Following this, the average spectrum for the selected ROI was calculated. The spectral processing involved transforming the reflectance data into absorbance spectra using a logarithmic transformation. To improve the quality of the signal, denoising was performed using a second derivative Savitzky-Golay filter, with a polynomial order of two and a window length of 51. This step was essential to minimize noise and remove baseline while preserving the critical features of the spectral data for accurate analysis. For the data analysis, the amplitude of the absorbance peaks was identified, especially for those peaks at 1200 nm and 1430 nm, which are associated with OH bonds [25].

For quantitative analysis, 100 pixels were selected from each image as shown in Fig. 2 (b). The resulting matrices contained 100 spectra per measurement day for each neonate. The spectral processing followed a similar approach to that used in the previous step. However, in this step, only 121 wavelengths were included, as the beginning and end of the spectrum were noisy. The selected wavelengths range from 1105 to 1527 nm. Logarithmic transformation was then applied, followed by denoising using a second derivative Savitzky-Golay filter, with a polynomial order of two and a window length of 25. Finally, median centring was performed.

As standard clinical features were not available for all consecutive days in neonates being assessed, interpolation was used to fill in the missing values.

The response vector Y was created based on the visual medical assessment and the neonate's weight. If the weight remained the same or increased over time, it was considered an indication of possible oedema, while a decreasing weight suggested no oedema. A value of 0 was assigned for no oedema and 1 for oedema.

Overall, four datasets were created and used to develop the classification models, as shown in Fig. 3. Dataset 1 contained only spectral data, whereas Datasets 2 and 3 incorporated both sets of spectral and standard clinical features. Specifically, Dataset 2 included weight, birth weight, percentage fluid overload (Eq. (1), fluid input and fluid output, while Dataset 3 included only weight, birth weight and percentage fluid overload (Eq. (1). Weight gain or loss is the most used clinical and objective method for oedema detection. The goal was to determine whether spectral data alone could effectively predict oedema or if including clinical features would enhance model performance. Furthermore, PCA was applied to each dataset as a dimensionality reduction technique. Finally, Dataset 4 contained only standard clinical features and served as the baseline. Datasets 1, 2, 3 and 4 were used to develop Models 1, 2, 3 and 4, respectively.

2.4. Spectral and statistical analysis

Initially, qualitative analysis was performed, comparing the mean spectrum from neonates with oedema and the neonates without oedema, during different days of measurement. Also, increase or decrease in light

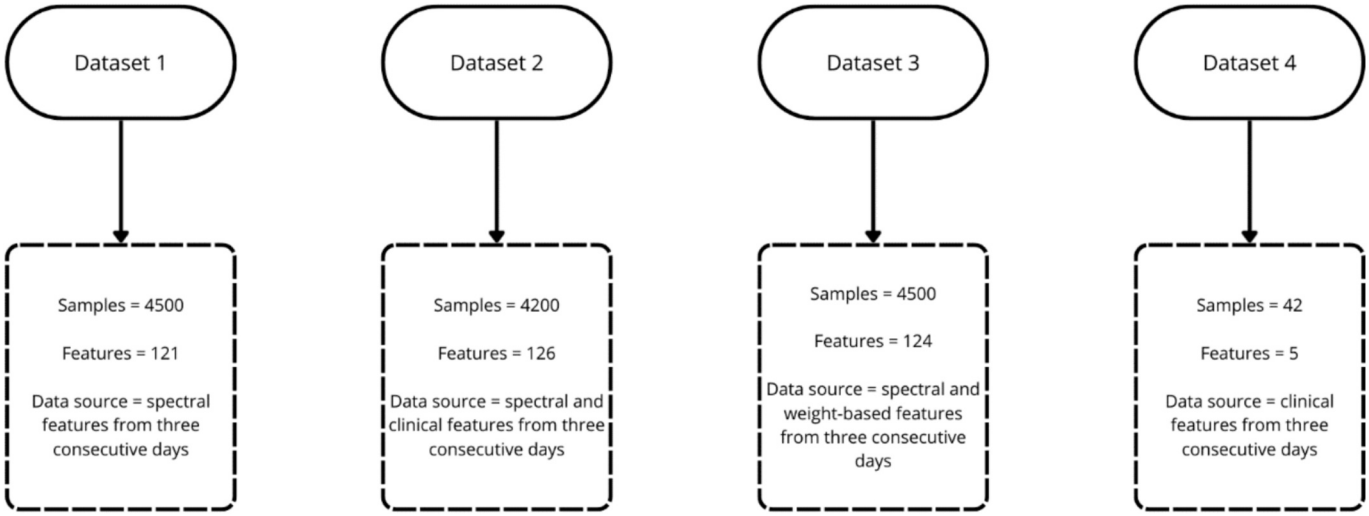

Fig. 3. Datasets created using spectral and standard clinical features from neonates over three consecutive days. Samples refers to the number of observations included in the dataset, while features refers to the variables or measured characteristics (e.g., spectral points or clinical features) used as inputs for model development.

absorption at water-sensitive bands was calculated. A Mann-Whitney *U* test was used for significance testing between both groups.

In clinical practice and some research studies, a weight-based formula is applied to determine if a neonate has oedema or not. Simple linear regression was used to find a relation between the formula and spectral features.

$$\%FluidOverload = \frac{Dailyweight - birthweight}{Birthweight} \times 100 \quad (1)$$

Additionally, Partial Least Squares-Discriminant Analysis (PLS-DA) was performed using Datasets 1,2 and 3 (Fig. 3) after applying PCA. PLS-DA is a supervised classification method that extends PLS regression by maximizing the separation between predefined classes. However, due to its susceptibility to overfitting, particularly with small sample sizes, cross-validation (CV) is essential [28]. To evaluate model performance, several metrics were reported: sensitivity, specificity, F1 score, accuracy, and Root Mean Square Error of Cross-Validation (RMSECV), along with the mean and standard deviation of validation results. Confusion matrices were also included, featuring recall and precision scores for the test sets. As noted in [29], these metrics are especially valuable when working with limited datasets.

Furthermore, to establish a baseline, a model was trained using the standard clinical features contained in Dataset 4. Because PLS-DA is primarily designed for high-dimensional data, its application to Dataset 4 would introduce unnecessary complexity. In this context, logistic regression represents a more appropriate choice. Logistic regression was therefore implemented, with optimal parameters determined through grid search (Table 1).

The datasets were divided into training and testing sets, ensuring a well-balance distribution of neonates with and without oedema in each set. There was no overlap between patients in the training and test sets. The training set included 10 patients (6 with signs of oedema and 4 without), while the test set consisted of 5 neonates (3 with signs of oedema and 2 without). For the PLS-DA models, within the training set, venetian blinds cross-validation, with 40 splits and a blind thickness of 1, was applied to the spectral samples to evaluate model consistency. No spectra from test set neonates were included in the training or cross-validation folds. Each day was treated as an independent sample to increase the effective dataset size. Although Leave-One-Patient-Out cross-validation is a valid option for small datasets, it was not considered since it does not provide a fully independent test set and it tends to be overly optimistic for evaluating model performance, particularly in datasets with high correlated samples [30]. In contrast, logistic regression employed stratified k-fold cross-validation with 5 splits. The PLS toolbox in MATLAB was used for building the models and further analysis.

Table 1
Parameter grid for logistic regression model tuning.

Parameters	Values
'penalty'	['l1','l2',None]
'C'	[0.01, 0.1, 1]
'class weight'	[None, 'balanced']
'solver'	['liblinear', 'saga']

3. Results

3.1. Data collection

In total 20 patients were recruited, however five were discharged from the unit before the study could be completed. Median and interquartile range (IQR) of gestational age, birth weight, and age at study by oedema status are summarized in Table 2. From the 15 neonates with data from three consecutive days, six did not have clinical signs of oedema, compared to nine with oedema.

Furthermore, Fig. 4 illustrates the setup used for data acquisition, including the positioning of the equipment and its integration into the clinical environment. It is important to note that some challenges were encountered during data collection. Low birth weight neonates were not included, mainly as the equipment did not fit under the incubators used for very small or preterm infants. In certain cases, the neonates were unsettled, which may have introduced movement-related variability into the measurements. Additionally, the room was occasionally exposed to excessive ambient light, potentially affecting the spectral data by altering light conditions during the recording process. The entire

Table 2
Median and Interquartile Range (IQR) of gestational age, birth weight, and age at study by oedema status.

	Oedema group		No oedema group	
	Median	IQR	Median	IQR
Gestational age (weeks)	38.00	34.00 to 38.40	37.70	35.93 to 39.10
Birth weight (kg)	2.80	2.09 to 3.06	3.08	2.40 to 3.26
Age at study (days)	11.00	7.00 to 63.00	16.00	14.25 to 27.00

Fig. 4. Data acquisition set up in the neonatal intensive care unit.

setup and measurement process took approximately 5 to 7 min to complete.

3.2. Spectral analysis

As shown in Fig. 5 (a), the second derivative spectra of neonates with and without oedema can be differentiated from the first day of measurement, particularly by the minima bands related to OH bonds around 1190 nm and 1430 nm. These bands correspond closely to the absorption of water within the skin, which are typically found near 1200 nm and 1450 nm [25]. In neonates with oedema, the peaks appeared higher in amplitude compared to those without oedema. Despite these differences, the overall shape of the spectra remained similar. Although the hyperspectral camera covers a range from 900 to 1700 nm and should, in theory, capture the 970 nm band, this band was not clearly visible due to device limitations and noise interference.

Furthermore, Fig. 5 (b) compares the oedema and non-oedema spectra on days 1 and 3. In the oedema condition, the water content on day 3 was higher than on day 1. In contrast, as expected, in non-oedematous infants there was a decrease in water content from day 1 to day 3. A statistically significant difference was found between oedema and non-oedema groups, in the percentage change of light absorbance at 1200 nm between day 1 and day 3, indicating that tissue in the oedematous group had an increase in water content (10.09 %) compared to the non-oedematous group (−9.31 %) over the three-day period ($p = 0.012$). No significant difference was found in light absorbance at 1430 nm.

3.3. Statistical analysis

In total, data from 15 neonates were collected over three consecutive days, which were used to create the datasets. Note that Dataset 2 (Fig. 3) has a different size because one neonate had missing fluid data and was therefore excluded from this dataset. PLS-DA models were built using the principal components (PCs) obtained from each dataset. The optimal number of PCs for each model was determined based on the explained variance as shown in Fig. 6. For Dataset 1, five PCs were selected, accounting for 80.51 % of the total variance. In contrast, Datasets 2 and 3 each utilized eight PCs, explaining 81.22 % and 81.56 % of the variance,

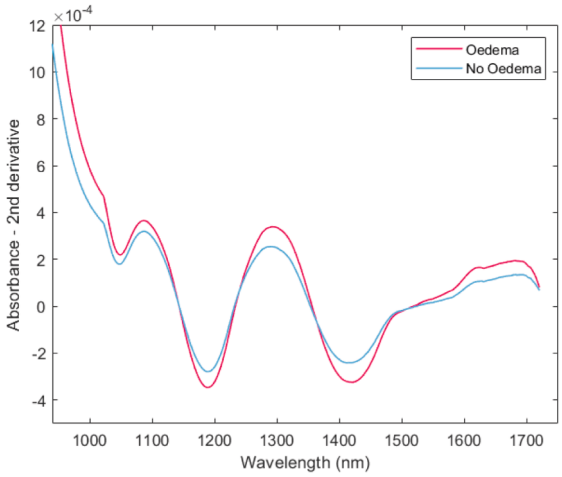

(a)

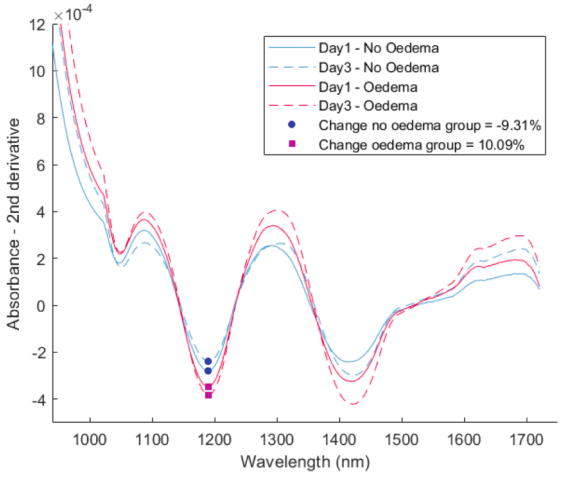

(b)

Fig. 5. (a) Mean second derivative spectra for day 1 from neonates clinically oedematous and non-oedematous, acquired in the range of 900 – 1700 nm. (b) Mean second derivative spectra for day 1 and day 3 of testing from neonates clinically oedematous and non-oedematous, acquired in the range of 900 – 1700 nm.

respectively. Additionally, the optimal number of latent variables (LVs) for each model was determined through cross-validation, using RMSECV as the selection criterion. As shown in Fig. 7, two LVs were selected for each model based on their corresponding RMSECV values.

Furthermore, the loading of the first PC was found to align closely with the spectrum of the second derivative of water, as illustrated in Fig. 8. The water peak is typically found around 1450 nm; however, in human skin, it has been reported to occur around 1437 nm [25]. When the second derivative is applied, a shift to the left is observed in both cases. This suggests that the primary factor distinguishing between oedema, or no oedema conditions is water content. Additionally, in models that include standard clinical features, the weight-based formula stands out as the main contributor to variance among all clinical features.

To visualize oedema clustering, the classification of oedema and no oedema groups for each model is presented in the PLS-DA score plots in Fig. 9, shown as projections of LVs. The x-axis represents latent variable 1 (LV1), while the y-axis represents latent variable 2 (LV2). The plots reveal two clusters, though some overlap is present. Model 1 and Model

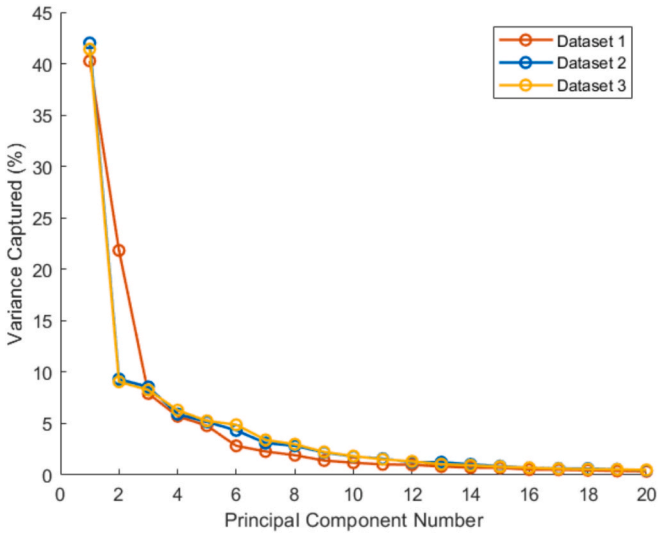

Fig. 6. Variance captured by each principal component for Datasets 1, 2, and 3.

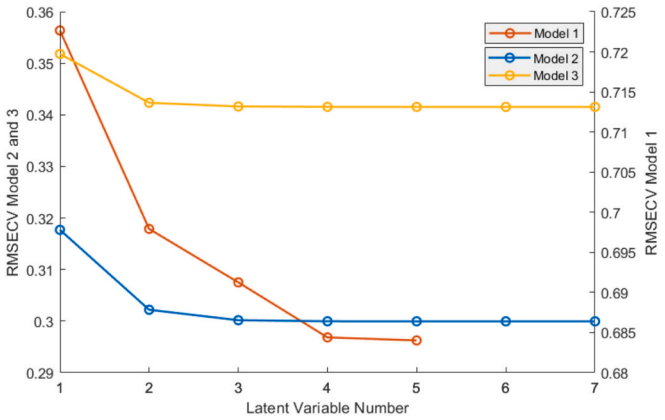

Fig. 7. RMSECV of the models.

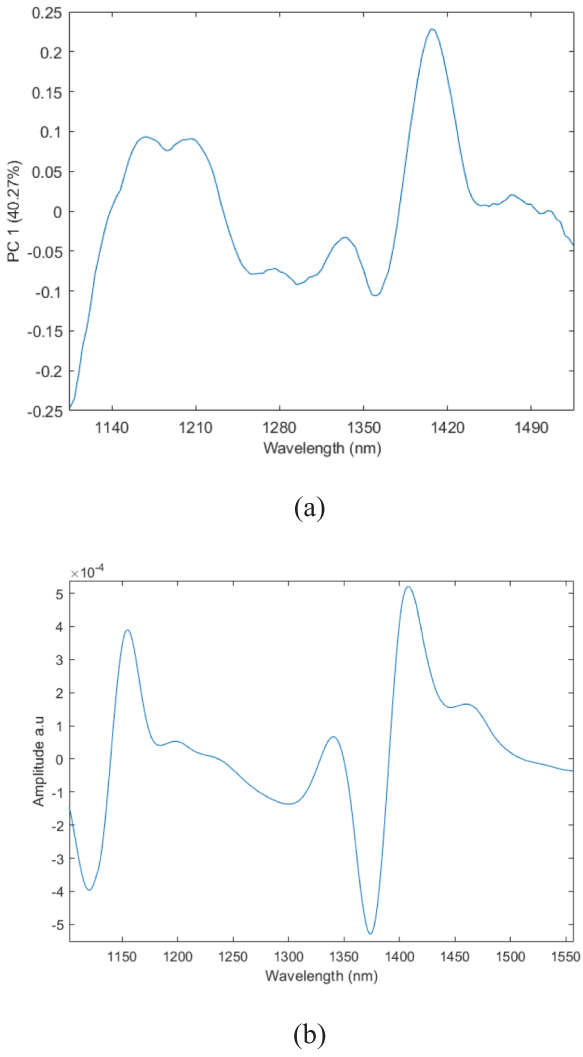

Fig. 8. (a) Loading of the first principal component. (b) Second derivative of pure water.

3, demonstrated clear clustering, whereas Model 2, had a few oedema points appear within the no-oedema group. Since Model 1 and Model 3 do not include fluid data, unlike Model 2, the observed overlap may be due to some neonates undergoing diuretic therapy. However, assessing model performance based solely on score plots is insufficient; a more in-depth analysis is necessary.

Table 3 presents the performance of the three PLS-DA models on the training sets, evaluated using 40-fold venetian blinds cross-validation. Model performance was assessed based on sensitivity, specificity, F1 score, accuracy and RMSECV, with results reported as mean ± standard deviation. Given the class imbalance in binary classification, the F1 score provides a more comprehensive measure of performance. Additionally, Table 4 summarizes the models performance on new data, showing testing results using the same evaluation metrics.

Model 1 demonstrated a balanced and stable performance across both cross-validation and testing evaluations, making it a strong alternative. The consistency of its F1 score suggested that it maintains reliability across different datasets. Model 2 on the other hand, showed a decline in testing performance, indicating potential overfitting. The drop in F1 score from 87.60 % ± 4.40 % to 82.64 % and 90.46 % ± 3.30 % to 83.72 %, between cross-validation and testing, suggested that while the model performed well during training, it struggled with real-world data, leading to unreliable classification. Model 3 exhibited the best generalization capability. The improvement in F1 score from 80.30 % ± 6.27 % to 90.23 % and 87.50 % ± 3.67 % to 92.22 % during testing highlights its strong generalization, making it the most robust and consistent performer among the three models. Additionally, ROC curves and AUC values were computed, and the results are available in the supplementary material (See supplementary material).

Furthermore, since each model was evaluated on the previously defined test sets, Table 5 provides a confusion matrix summarizing recall and precision values. According to the table, Model 1 did not misclassify No Oedema cases, however its false negatives were relatively high, leading to more missed oedema cases. Model 2 struggled with false negatives, leading to lower overall performance. In contrast, Model 3 yielded the fewest false negatives and no false positives, achieving the highest recall (85.56 %) and precision (100 %). These results aligned with the findings in Table 2 and Table 3, confirming that Model 3 outperformed the other two models.

Overall, Model 3 outperformed the others across all parameters, particularly in F1 score for both cross-validation and testing results, as well as in recall and precision. Including weight, birth weight and the formula based on those two variables enhanced Model 3's performance compared to Model 1, which only included spectral data. On the other hand, incorporating fluid data in Model 2 negatively impacted the model's performance on unseen data. This may be due to a lack of a strong correlation between fluid data and the presence of oedema.

Additionally, Table 6 presents the performance of a model trained

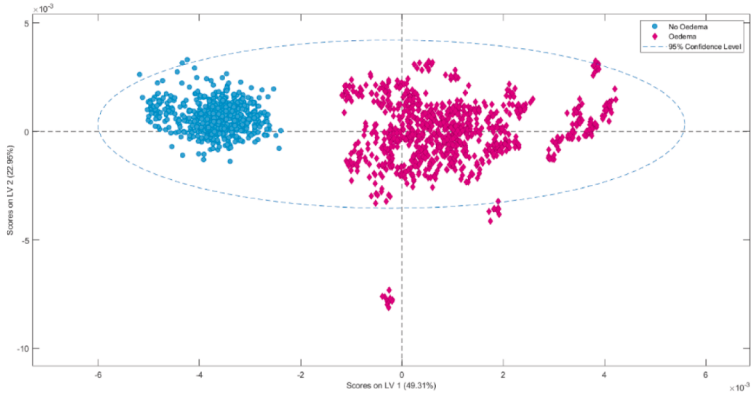

(a)

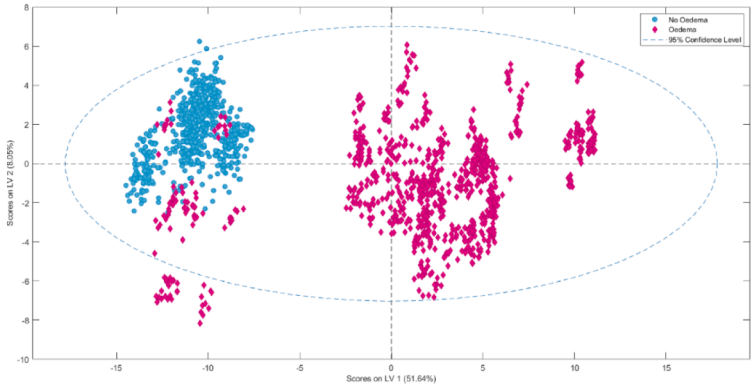

(b)

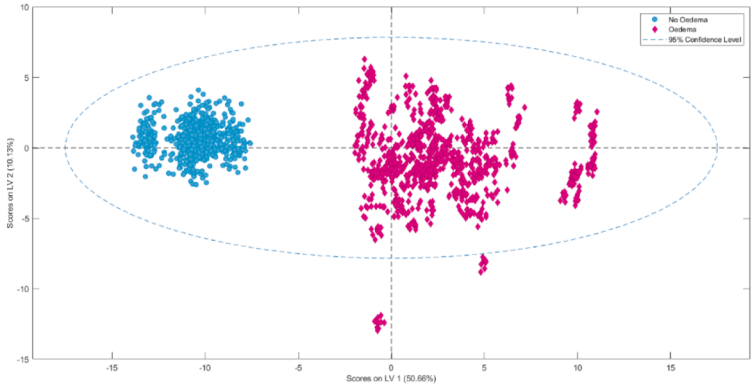

(c)

Fig. 9. PLS-DA score plots (a) Model 1. (b) Model2. (c) Model 3. Each point in the score plot represents a single spectral measurement projected onto the space of the principal components used for PLS-DA model training.

and tested exclusively on standard clinical features (Model 4). While training performance appeared high (overall accuracy 88.67 %), the large standard deviations in sensitivity, specificity, and F1 scores (ranging from 13.33 – 26.67 %) indicate considerable variability across folds. Testing results were substantially lower, with sensitivity 50.00 %, specificity 44.44 %, F1 score 42.86 %, and overall accuracy 46.67 %. These findings indicate that clinical features alone are insufficient to predict oedema status in critically ill neonates, as the clinical-only model performed worse than models incorporating spectral data.

Finally, linear regression was conducted between the percentage of fluid overload formula and the light absorbance at 1200 nm and 1430 nm. However, when using data from all three days, the R^2 values were 0.28 and 0.15 for the absorbances at 1200 nm and 1430 nm, respectively. Additionally, Fig. 10 shows the linear relationship between fluid

Table 3
Evaluation metrics (Mean ± SD) for PLS-DA models on training sets using Cross-Validation.

Model	Class	Sensitivity (M% ± SD%)	Specificity (M% ± SD%)	F1 Score (M% ± SD%)	Accuracy (M% ± SD%)	RMSECV (M ± SD)
Model 1	No Oedema	76.17 ± 8.96	89.28 ± 4.12	79.04 ± 5.88	84.03 ± 4.09	0.35 ± 0.03
	Oedema	89.28 ± 4.12	76.17 ± 8.96	87.06 ± 3.14		
Model 2	No Oedema	85.92 ± 5.94	91.88 ± 4.46	87.60 ± 4.40	89.23 ± 3.78	0.30 ± 0.03
	Oedema	91.88 ± 4.46	85.92 ± 5.94	90.46 ± 3.30		
Model 3	No Oedema	78.42 ± 8.47	88.94 ± 4.35	80.30 ± 6.27	84.73 ± 4.65	0.34 ± 0.03
	Oedema	88.94 ± 4.35	78.42 ± 8.47	87.50 ± 3.67		

Table 4
Evaluation metrics for PLS-DA models on testing sets.

Model	Class	Sensitivity (%)	Specificity (%)	F1 Score (%)	Accuracy (%)
Model 1	No Oedema	100.00	85.22	90.02	91.13
	Oedema	85.22	100.00	92.02	
Model 2	No Oedema	100.00	72.00	82.64	83.20
	Oedema	72.00	100.00	83.72	
Model 3	No Oedema	100.00	85.56	90.23	91.33
	Oedema	85.56	100.00	92.22	

Table 5
Confusion matrix for PLS-DA models on testing sets.

Model 1		No Oedema	Oedema	Recall (%)
8LV	Predicted as No Oedema	600	133	85.22
	Predicted as Oedema	0	767	
	Precision (%)	100.00		
Model 2		No Oedema	Oedema	Recall (%)
3LV	Predicted as No Oedema	600	252	72.00
	Predicted as Oedema	0	648	
	Precision (%)	100.00		
Model 3		No Oedema	Oedema	Recall (%)
3LV	Predicted as No Oedema	600	130	85.56
	Predicted as Oedema	0	770	
	Precision (%)	100.00		

Table 6
Optimal parameters found by grid search and evaluation metrics for logistic regression model on training and testing sets for Model 4.

Best values found	'penalty': 'l1'	'C': 1	'class weight': None	'solver': 'liblinear'
Class	Sensitivity (M% ± SD %)	Specificity (M% ± SD %)	F1 Score (M% ± SD%)	Accuracy (M% ± SD%)
No Oedema	93.33 ± 13.33	86.67 ± 26.67	89.33 ± 13.73	88.67 ± 15.72
Oedema	86.67 ± 26.67	93.33 ± 13.33	87.14 ± 19.38	
Class	Sensitivity (%)	Specificity (%)	F1 Score (%)	Accuracy (%)
No Oedema	50.00	44.44	42.86	46.67
Oedema	44.44	50.00	50.00	

overload and absorbance at 1200 nm and 1430 nm.

4. Discussion and conclusions

To the best of our knowledge, this is the first study to use an optical technique to detect and monitor oedema in critically ill neonates. The ability to detect oedema using hyperspectral measurements is based on the spectral differences observed between oedematous and non-oedematous tissue, which arise due to various physiological changes, particularly increased water content. These changes affect the reflected light after it interacts with tissue, resulting in spectral features that are indicative of oedema, particularly when observed at water-related wavelengths such as 1200 nm and 1450 nm.

These findings align with those of Budylin et al. [31], where oedema conditions were characterized by an increase in water content, as evidenced by elevated absorbance in the water-related bands at 970 nm and 1200 nm, measured through diffuse reflectance spectroscopy and multispectral imaging. However, their study was conducted on adult healthy volunteers, with oedema induced in specific areas and measured at various time points on the same day after induction, whereas the optical characteristics of neonatal skin differ. Specifically, the optical penetration depth in tissue depends on both scattering and absorption properties. In neonatal skin, scattering is generally lower than in adult skin due to its thinner epidermis and dermis, higher water content, and reduced collagen density [32]. Nevertheless, the pronounced increase in water absorption beyond 1100 nm significantly limits light penetration at these longer wavelengths. Consequently, even with reduced scattering, spectral features above 1100 nm in neonatal skin primarily represent superficial layers, while those near 970 nm capture contributions from relatively deeper tissue regions.

Additionally, weight and fluid balance are not reliable indicators for detecting or monitoring oedema. Formulas based on these variables do not directly account for water content within the tissue. Both fluid balance-based and weight-based approaches may have inaccuracies [6]. As described in studies on neonates, the agreement between fluid balance and daily weight change is poor 33,34, indicating that fluid balance charts may be inaccurate in critically ill newborns. In some cases, the discrepancy between recorded fluid balance and actual weight change exceeded 20 % [34].

The correlations observed using the weight-based formula confirmed the poor agreement between weight and oedema status using a simple linear regression. Weight is the most used variable in research to assess fluid status [35–37]. However, it can reflect fat mass growth rather than just water. Moreover, patients with increased severity of illness are less likely to be weighed in neonatal wards [33]. Overall, standard clinical features alone do not provide an accurate result for oedema classification, as demonstrated by Model 4, which showed large standard deviations during cross-validation and poor performance on the test set (Table 6). However, integrating spectral data from the skin in the near-infrared region could potentially yield more reliable results.

Finally, PLS-DA proves to be a suitable classification method for this condition. The most relevant band, according to the loadings, appears to be the one related to water absorbance around 1430 nm. The most relevant clinical features for predicting oedema are weight-related factors, such as weight on the day of the measurement, birth weight and the formula derived from these two variables. On the other hand, visually, the 1200 nm peak appears to carry the most information for distinguishing the presence of oedema. However, PLS-DA offers a more in-depth analysis of features that are not immediately apparent.

The PLS-DA score plots revealed two identifiable clusters corresponding to oedema and no-oedema neonates. However, metrics such as confusion matrices and F1 scores are necessary to determine the model's effectiveness in classifying oedema cases.

Based on the PLS-DA models, Model 1 and Model 3 performed the best, particularly when examining the F1 score (see Table 3 and Table 4)

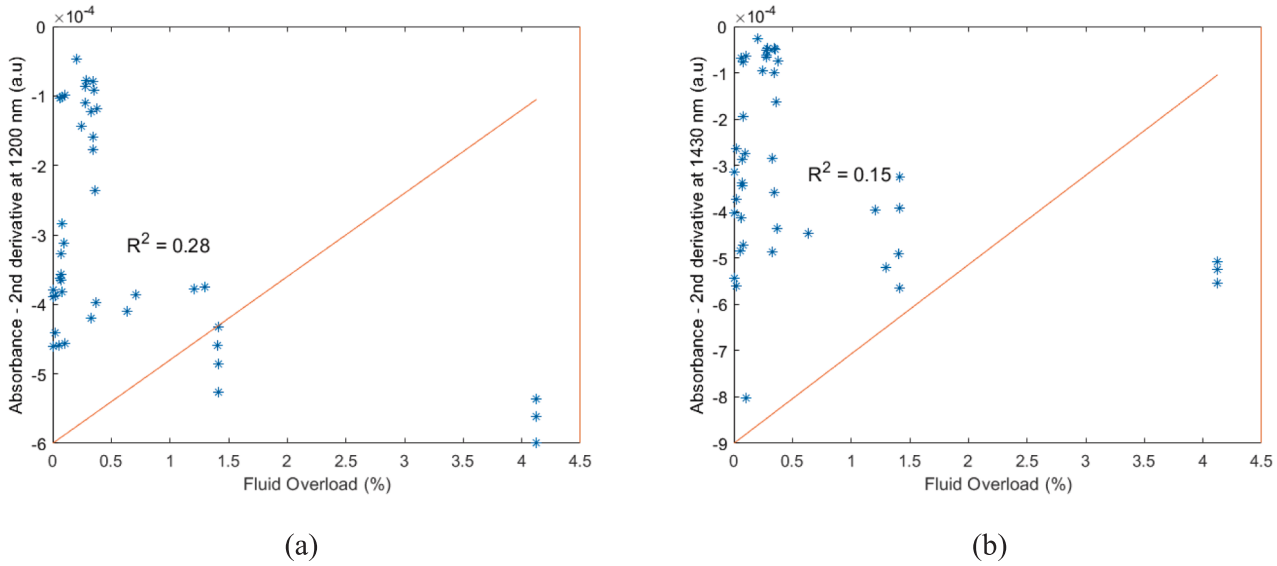

Fig. 10. Scatter plots showing the linear relationship between fluid overload and absorbance at a) 1200 nm and b) 1430 nm.

and confusion matrix (see Table 5). Using only spectral data, in the range from 970 nm to 1700 nm, produced reliable results (Model 1). However, combining spectral data with weight- based data resulted in a robust model (Model 3). Conversely, incorporating fluid input and output data led to the poorest performance (Model 2), confirming that fluid data is not strongly correlated with oedema.

We acknowledge the following limitations of our study: insensible water loss was not considered in the fluid recorded data and is very difficult to assess. The sample size was small, but this was part due to the difficulties in measuring unwell infants on consecutive days and those who were not very sick, and probably not oedematous, not staying on the neonatal unit for three days. Low birth weight neonates were not included, mainly as the equipment did not fit under the incubators used for very small or preterm infants.

A limitation of this study is that repeated measurements obtained from the same neonate on different days were treated as independent samples in the classification model. This assumption was made to increase the effective dataset size, given the limited number of subjects available in this feasibility study. While this approach enabled initial exploration of the potential of NIRS for oedema status assessment, it may lead to an overestimation of statistical significance due to the lack of within-subject correlation control. Future studies with larger cohorts will be designed to incorporate repeated-measures or mixed-effects models, which can more appropriately account for intra-individual variability. However, the present findings serve as an important proof-of-concept demonstration of the feasibility of this optical technique in neonatal oedema monitoring.

Further research is needed to determine whether incorporating more clinical features can enhance the model or even predict oedema with just a single day's measurement. Future work should focus on predicting the neonate's status using only data from one day of measurement, which would enable more rapid medical decisions and timely treatment. Real-time application of this method is feasible; an algorithm could be developed based on the current workflow, with automated ROI selection being a key step. In addition, improving sensor performance and calibration will be essential to enhance signal fidelity and spectral accuracy, while also addressing potential confounding factors such as skin pigmentation, motion artifacts, and environmental light, thereby further improving measurement reliability. This would support medical decision-making regarding the presence or absence of oedema in a patient. Furthermore, investigating other spectral bands, as well as shape variations or shifts associated with oedema, could provide valuable insights.

CRediT authorship contribution statement

Mariana Castro-Montano: Writing – review & editing, Writing – original draft, Visualization, Validation, Software, Project administration, Methodology, Investigation, Formal analysis, Data curation, Conceptualization. **Andy Petros:** Writing – review & editing, Resources. **Ling Li:** Writing – review & editing, Validation, Supervision, Conceptualization. **Enayetur Rahman:** Writing – review & editing, Validation. **Simon Hannam:** Writing – review & editing, Resources. **Grant Clow:** Resources. **Panayiotis A Kyriacou:** Writing – review & editing, Validation, Supervision, Conceptualization. **Jim McLaughlin:** Writing – review & editing, Resources. **Meha Qassem:** Writing – review & editing, Validation, Supervision, Project administration, Methodology, Conceptualization.

Funding

This research did not receive any specific grant from funding agencies in the public, commercial, or not-for-profit sectors.

Declaration of competing interest

The authors declare that they have no known competing financial interests or personal relationships that could have appeared to influence the work reported in this paper.

Appendix A. Supplementary data

Supplementary data to this article can be found online at https://doi.org/10.1016/j.bspc.2025.109444.

Data availability

Data underlying the results presented in this paper are not publicly available at this time but may be obtained from the authors upon reasonable request.

References

[1] D.T. Selewski, et al., The impact of fluid balance on outcomes in premature neonates: a report from the AWAKEN study group, Pediatr. Res. 87 (3) (Feb. 2020) 550–557, https://doi.org/10.1038/S41390-019-0579-1.

[2] P.J. Shah, Perioperative fluid management and blood transfusion in newborns and neonates, Clinical Anesthesia for the Newborn and the Neonate, pp. 439–455, Jan. 2023, doi: 10.1007/978-981-19-5458-0_23/TABLES/13.

[3] A. Tobias, B.D. Ballard, S.S. Mohiuddin, Physiology, water balance, StatPearls, Oct. 2022, Accessed: Feb. 06, 2024. [Online]. Available: https://www.ncbi.nlm.nih.gov/books/NBK541059/.

[4] D. Chawla, R. Agarwal, A.K. Deorari, V.K. Paul, Fluid and electrolyte management in term and preterm neonates, Indian J. Pediatr. 75 (3) (Mar. 2008) 255–259, https://doi.org/10.1007/S12098-008-0055-0/METRICS.

[5] M.D.B.B. Méio, M.E.L. Moreira, Total Body Water in Newborns, Handbook of Anthropometry: Physical Measures of Human Form in Health and Disease, 1121–1135, Jan. 2012, doi: 10.1007/978-1-4419-1788-1_67.

[6] L.J. Weaver, C.P. Travers, N. Ambalavanan, D. Askenazi, Neonatal fluid overload—ignorance is no longer bliss, Pediatr. Nephrol. 38 (1) (Jan. 2023) 47, https://doi.org/10.1007/S00467-022-05514-4.

[7] F.A.M. Steven E. Lucking, Pediatric Critical Care. Springer International Publishing, 2021. doi: 10.1007/978-3-030-53363-2.

[8] A.K.C Leung, W.L.M. Robson Alexander, K.C. Leung, W.L.M. Robson, P. of Paediatricts, A.K.C. Leung, Oedema in childhood, https://doi.org/10.1177/146642400012000407, 120, 4, 212–219, Dec. 2000, doi: 10.1177/146642400012000407.

[9] "Wound Essentials 4: Chronic oedema – the importance of skin care – Wounds UK." Accessed: Nov. 28, 2024. [Online]. Available: https://wounds-uk.com/wound-essentials/wound-essentials-4-chronic-oedema-the-importance-of-skin-care/.

[10] P.H.T. Cartlidge, N. Rutter, Serum albumin concentrations and oedema in the newborn, Arch. Dis. Child. 61 (7) (Jul. 1986) 657–660, https://doi.org/10.1136/ADC.61.7.657.

[11] G.J. Schwartz, M. Rashid, Overview, structure, and function of the nephron, Pediatric Crit. Care (2021) 863–909, https://doi.org/10.1007/978-3-030-53363-2_29.

[12] L. Gordon et al., Approaches to evaluation of fluid balance and management of fluid overload in neonates among neonatologists: a Neonatal Kidney Collaborative survey, J. Perinatol. 2023 43:10, 43, 10, 1314–1315, Jul. 2023, doi: 10.1038/s41372-023-01738-w.

[13] B.J. Farr, L.J. Bechard, S.E. Rice-Townsend, N.M. Mehta, Bio-impedance spectroscopy for total body water assessment in pediatric surgical patients: a single center pilot cohort study, J. Pediatr. Surg. 57 (12) (Dec. 2022) 962–966, https://doi.org/10.1016/J.JPEDSURG.2022.07.014.

[14] W. Tang, D. Ridout, N. Modi, Assessment of total body water using bioelectrical impedance analysis in neonates receiving intensive care, Arch. Dis. Child. Fetal. Neonatal Ed. 77 (2) (Sep. 1997) F123–F126, https://doi.org/10.1136/FN.77.2.F123.

[15] M. Allinovi, M. Saleem, P. Romagnani, P. Nazerian, W. Hayes, Lung ultrasound: a novel technique for detecting fluid overload in children on dialysis, Nephrol. Dial. Transplant. 32 (3) (Mar. 2017) 541–547, https://doi.org/10.1093/NDT/GFW037.

[16] D.B. Kantor, et al., Fluid balance is associated with clinical outcomes and extravascular lung water in children with acute asthma exacerbation, Am. J. Respir. Crit. Care Med. 197 (9) (May 2018) 1128–1135, https://doi.org/10.1164/RCCM.201709-1860OC/SUPPL_FILE/DISCLOSURES.PDF.

[17] D.M. Ferreira, M.N. Souza, Bioelectrical impedance spectroscopy for the assessment of body fluid volumes of term neonates, Braz. J. Med. Biol. Res. 37 (11) (2004) 1595–1606, https://doi.org/10.1590/S0100-879X2004001100002.

[18] A. Bosy-Westphal, et al., Need for optimal body composition data analysis using air-displacement plethysmography in children and adolescents, J. Nutr. 135 (9) (Sep. 2005) 2257–2262, https://doi.org/10.1093/JN/135.9.2257.

[19] S. Heymsfield, J.D. Bell, D. Heber, Phenotyping, body composition, and precision nutrition, Precision Nutrition: the Science and Promise of Personalized Nutrition and Health, pp. 143–152, 2024, 10.1016/B978-0-443-15315-0.00008-0.

[20] B.S. Zemel, Body composition during growth and development, Human Growth and Development, pp. 461–486, Jan. 2012, doi: 10.1016/B978-0-12-383882-7.00018-0.

[21] B.E. Lingwood, Bioelectrical impedance analysis for assessment of fluid status and body composition in neonates–the good, the bad and the unknown, Eur. J. Clin. Nutr. 67 (Suppl 1) (2013) S28–S33, https://doi.org/10.1038/EJCN.2012.162.

[22] K. Okubo, "NIR Hyperspectral Imaging," Transparency in Biology: Making the Invisible Visible, pp. 203–222, Jan. 2020, doi: 10.1007/978-981-15-9627-8_10/FIGURES/7.

[23] A. Holmer, et al., Oxygenation and perfusion monitoring with a hyperspectral camera system for chemical based tissue analysis of skin and organs, Physiol. Meas. 37 (11) (Oct. 2016) 2064, https://doi.org/10.1088/0967-3334/37/11/2064.

[24] M. Mamouei, S. Chatterjee, M. Razban, M. Qassem, P.A. Kyriacou, Design and analysis of a continuous and non-invasive multi-wavelength optical sensor for measurement of dermal water content, Sensors (Basel) 21 (6) (Mar. 2021) 1–12, https://doi.org/10.3390/S21062162.

[25] A.N. Bashkatov, E.A. Genina, V.I. Kochubey, V.V. Tuchin, Optical properties of human skin, subcutaneous and mucous tissues in the wavelength range from 400 to 2000 nm, J. Phys. D Appl. Phys. 38 (15) (Jul. 2005) 2543, https://doi.org/10.1088/0022-3727/38/15/004.

[26] G.N. Stamatas, M. Southall, N. Kollias, In vivo monitoring of cutaneous edema using spectral imaging in the visible and near infrared, J. Invest. Dermatol. 126 (8) (Aug. 2006) 1753–1760, https://doi.org/10.1038/SJ.JID.5700329.

[27] M. Qassem, P.A. Kyriacou, Comparing the rates of absorption and weight loss during a desorption test using near infrared spectroscopy, Skin Res. Technol. 19 (2) (May 2013) 137–144, https://doi.org/10.1111/SRT.12024.

[28] J.A. Westerhuis, et al., Assessment of PLSDA cross validation, Metabolomics 4 (1) (Mar. 2008) 81–89, https://doi.org/10.1007/S11306-007-0099-6/FIGURES/5.

[29] I. Iqbal, G.A. Odesanmi, J. Wang, L. Liu, Comparative investigation of learning algorithms for image classification with small dataset, Appl. Artif. Intell. 35 (10) (Aug. 2021) 697–716, https://doi.org/10.1080/08839514.2021.1922841.

[30] J. Ezenarro, D. Schorn-García, How are chemometric models validated? A systematic review of linear regression models for NIRS data in food analysis, J. Chemom. 39 (6) (May 2025) e70036, https://doi.org/10.1002/CEM.70036.

[31] G.S. Budylin, et al., In vivo sensing of cutaneous edema: a comparative study of diffuse reflectance, Raman spectroscopy and multispectral imaging, J. Biophotonics 15 (1) (Jan. 2022) e202100268, https://doi.org/10.1002/JBIO.202100268.

[32] A.P. Miller, F.H. Mustafa, P.W. Jones, H.E. Jeffery, A.E. Carberry, A.L. McEwan, Near-infrared spectroscopy to monitor nutritional status of neonates: a review, IEEE Rev. Biomed. Eng. 13 (2020) 280–291, https://doi.org/10.1109/RBME.2019.2951299.

[33] T.M. Neumayr, et al., Assessment of fluid balance after neonatal cardiac surgery: a description of intake/output vs. weight-based methods, Pediatr. Nephrol. 38 (4) (Apr. 2023) 1355–1364, https://doi.org/10.1007/S00467-022-05697-W/FIGURES/3.

[34] Y. Van Asperen, P.L. Brand, J. Bekhof, Reliability of the fluid balance in neonates, Acta Paediatr. 101 (5) (May 2012) 479–483, https://doi.org/10.1111/J.1651-2227.2012.02591.X.

[35] F.Y. Matsushita, V.L.J. Krebs, W.B. de Carvalho, Association between fluid overload and mortality in newborns: a systematic review and meta-analysis, Pediatr. Nephrol. 37 (5) (May 2022) 983–992, https://doi.org/10.1007/S00467-021-05281-8/FIGURES/6.

[36] D.T. Selewski et al., The impact of fluid balance on outcomes in critically ill near-term/term neonates: a report from the AWAKEN study group, Pediatr. Res. 2018 85:1, vol. 85, no. 1, pp. 79–85, Sep. 2018, doi: 10.1038/s41390-018-0183-9.

[37] M.L. Wright, B.G. Klamer, E. Bonachea, J.D. Spencer, J.L. Slaughter, T. H. Mohamed, Positive fluid balance and diuretic therapy are associated with mechanical ventilation and mortality in preterm neonates in the first fourteen postnatal days, Pediatr. Nephrol. 38 (7) (Jul. 2023) 2243–2253, https://doi.org/10.1007/S00467-022-05861-2/FIGURES/2.